Supplemental Information for

Dynamically assembled bionic ion pumps interface towards high-rate and cycling stable zinc metal batteries

Xiaoyun Xu, Songmei Li, Junwei An, Zicheng Luo, Juan Du, Jinyan Zhong, Mei Yu, Shubin Yang, Bin Li

This file includes:
Supplemental Figs. 1 to 38
Supplemental References

Methods

Materials

All chemicals were of analytical grade and used directly after purchase without further purification. Propanone, ethyl alcohol, urea, sodium dodecyl sulfate (SDS), sodium sulfide (Na_2S), acetic anhydride and zinc trifluoromethanesulfonate were purchased from aladdin.

Preparation of α-HP

α-HP was prepared by a reduction method. Firstly, wool fibers were soaked in acetone for 4 h and then washed three times with ethanol to remove oils and impurities. The washed wool fibers (5 g) were immersed in a 50 mL aqueous solution containing 8 M urea (24 g), 0.1 M SDS (1.5 g), 0.1 M Na_2S (0.8 g) and stirred at 60 °C for 8 h. The yellow crude keratin solution was obtained by filtration and dialyzed with dialysis bags (molecular weight cut-off of 3,500 D) in deionized water for 3 D to remove protein denaturant and reducing agents. During the dialysis process, the deionized water was replaced every 3 h, and the volume ratio of deionized water to dialysate was maintained at about 100:1. Finally, the above keratin solution was concentrated to 20 mL and freeze-dried to obtain white α-HP powder.

Preparation of α-HP$_{ace}$

Acetic anhydride was selected as the acetylating agent. A 1 g mL^{-1} solution of a-HP and a 0.1 mol L^{-1} solution of acetic anhydride were first prepared. Then the two solutions were mixed in a volume ratio of 1:1 and stirred at room temperature for 30 min. immediately followed by dialysis in deionized water using a dialysis bag (with a molecular weight cut-off of 3500 D) for 1 D to remove the by-product (CH_3COOH) and excess acetic anhydride. During the dialysis process, the deionized water was replaced every 3 h. The volume ratio of deionized water to dialysate was kept at about 100:1. Finally, the above protein solution was concentrated to 20 mL and freeze-dried to obtain the α-HP$_{ace}$ powder.

Preparation of electrolytes

2M $Zn(OTf)_2$ electrolyte: Zinc trifluoromethanesulfonate ($(CF_3SO_3)_2Zn$) is purchased from aladdin. 7.27 mg $(CF_3SO_3)_2Zn$ is added to 10 mL of deionized water and then stirred with a magnetic stirrer for 30 min to obtain a homogeneous solution. This homogeneous solution is the reference electrolyte 2M $Zn(OTf)_2$.

α-HP$_{ace}$@$Zn(OTf)_2$ electrolyte: α-HP$_{ace}$ is prepared by reduction and acetylation. A electrolyte (α-HP$_{ace}$@$Zn(OTf)_2$) for bionic ion pumps interface dynamically assembling is obtained by introducing α-HP$_{ace}$ into the 2M $Zn(OTf)_2$ electrolyte (the mass percentage of α-HP$_{ace}$ in the electrolyte is 0.5 wt.%).

Preparation of NaV_3O_8-1.5H_2O (NVO) cathode materials

Firstly, 1.753 g of NaCl and 1.000 g of V_2O_5 were added to 15 mL of deionized water and then stirred vigorously for 96 h in an airtight environment at 30°C. After that, the brick-red mixture was centrifuged at 5000 rpm for 5 mins for three times. Finally, the brick-red NaV_3O_8-1.5H_2O active material was obtained by freeze-drying.

70 wt.% of the NVO, 20 wt.% of the conductive carbon (Super P) and 10 wt.% of the binder polyvinylidene fluoride (PVDF) were mixed in N-Methylpyrrolidone (NMP) and ground for 30 min. Then, the obtained cathode slurry was coated onto the carbon paper by a simple blade coating method. Finally, the NVO cathodes were obtained by drying under vacuum at 70 °C for 12 h with an active material of about 2~5 mg cm^{-2}.

Material Characterizations

Zeta potential was used to characterize the electronegativity of acetylated proteins and interactions with Zn^{2+}. The contact angle of electrode was measured by an optical contact angle and interface tension meter (SL200KB, Kino, USA). X-ray diffraction (XRD D/MAX2200pc) with Cu-Kα1 radiation (λ=1.5406Å) was performed to identify the components and phase information of electrode surface. Atomic force microscope (AFM Dimension IconXR), fluorescence microscope and scanning electron microscope (SEM JSM7500 or JSM6010) were performed to observe the electrode surface morphology and protein self-assembly. Raman spectra and Fourier Transform infrared spectroscopy (FTIR Thermo Scientific Nicolet iS50) were performed to study chemical structure and property of the electrolyte. Elements valence information of anode surface was obtained by x-ray photoelectron spectroscopy (XPS Thermo Scientific K-Alpha). Time-of-flight secondary ion mass spectrometry (TOF-SIMS) was used to reveal the compositional distribution of SEIs. 3D microscope was used to study the morphology of the electrode surface after cycling.

Scanning Kelvin Probe (SKP) was used to characterise the evolution of the passivation layer in micro-regions on the electrode surface. SKP, a micro electrochemical technique, is used to characterize the electrochemical information on the surface of the specimens. The Gauss fitting formula is shown in following:

$$y = y_0 + \frac{A}{\sigma\sqrt{\frac{\Pi}{2}}} e^{-2\left(\frac{x-\mu}{\sigma}\right)^2}$$

where A is a constant, y_0 is the offset of the vertical axis, μ is the concentrated position of SKP potential distribution, σ is the degree of concentration of SKP potential distribution. The smaller the value of σ, the more concentrated the potential distribution is on the value of μ.

Calculation of cation ion transference number

The Zn||Zn and Zn@BIPI/α-HP_{ace}||Zn@BIPI/α-HP_{ace} symmetric cells were first assembled and then alternating-current (AC) impedance and direct-current (DC) potentiostatic polarization measurements were performed.

Before the potentiostatic polarization, this state is defined as the initial state and the corresponding interfacial impedance value is R_0. After 5000 s of electrostatic polarization, the trend of the response current tends to be stable. This state is defined as the stable state, and the corresponding interfacial impedance value is R_s. When the response current tends to be stable, AC impedance measurements are performed immediately to obtain the stable state Nyquist plots. Here, the semicircle of the Nyquist plot intersecting the Zre axis is the corresponding interfacial impedance value.

The cation transference number (t_+):

$$t_+ = \frac{\left(\frac{\Delta V}{I_0} - R_0\right)}{\left(\frac{\Delta V}{I_s} - R_S\right)}$$

where ΔV (10 mV) is the applied constant potential, I_0 is the initial response current, I_s is the steady-state response current, and R_0 and R_s are the electrode interface impedances before and after the polarization, respectively.

Calculation of activation energies (E_a)

The corresponding Zn^{2+} activation energies (E_a) were calculated based on the electrochemical impedance spectra (EIS) of the symmetric cell at different temperatures. According to the Arrhenius equation:

$$\frac{1}{R_{ct}} = A\exp\left(-\frac{E_a}{RT}\right)$$

Where R_{ct} is the interfacial resistance, A is the finger front factor, and E_a, R and T are the activation energy, molar gas constant and absolute temperature, respectively.

Electrochemical measurements

For the standardization of the measurements, all electrodes with a diameter of 10 mm were used in the assembly of the button cell, and 2M $Zn(OTf)_2$ or α-HP_{ace}@$Zn(OTf)_2$ electrolyte was used as the electrolyte, respectively. The reference group used 19 mm diameter glass fiber as the separator.

The Zn||Zn, Zn@BIPI/α-HP_{ace}||Zn@BIPI/α-HP_{ace}, Zn||Cu and Zn@BIPI/α-HP_{ace}||Cu cells were assembled using 2032 coin cells with 2M $Zn(OTf)_2$ or α-HP_{ace}@$Zn(OTf)_2$ electrolyte. In the symmetric cell test, the cells were cycled at 10 mA cm^{-2} and 1 mA cm^{-2} with a capacity of 1 mAh cm^{-2}. To eliminate the effect of uncertainties associated with the substrate (surface roughness and handling conditions) on subsequent cycling, coulombic efficiencies of the different electrolytes were measured in "mixed mode". All cell tests were performed on a CT2001A cell test instrument (LAND Electronic Co, BT2013A, China). Cyclic voltammetry (CV) analysis, linear scanning voltammetry (LSV) analysis, Tafel curve and electrochemical impedance spectroscopy (EIS) analysis were performed on an electrochemical workstation (CHI660E).

Full cells measurements

The Zn||NVO and Zn@BIPI/α-HP_{ace}||NVO full cells were assembled into a button cell (2032 button cell) with 2M $Zn(OTf)_2$ or α-HP_{ace}@$Zn(OTf)_2$ electrolyte. The full cell was cycled between 0.3 and 1.25 V at 5 A g^{-1} . The rate performance and full-cell performance were performed on a CT2001A cell test instrument (LAND Electronic Co, BT2013A, China). The full cell CV analysis was performed on an electrochemical workstation (CHI660E) with a scan rate of 1 mV s^{-1} and a scan range of 0.3 to 1.25 V.

The pouch cells were assembled with NVO cathode, Zn@BIPI/α-HP_{ace} anode and α-HP_{ace}@$Zn(OTf)_2$ electrolyte (4 × 5 cm). The pouch cells were cycled between 0.3 and 1.25 V at 1 A g^{-1}.

All cells are operated at an ambient temperature of 26°C.

Density Functional Theory (DFT) calculation

All DFT calculations were carried out by the Vienna Ab initio Simulation Package (VASP) program, and numerical simulations were performed using the projected augmented wave (PAW) method. The generalized gradient approximation (GGA) of Perdew-Burke-Ernzerhof (PBE) was used. In the geometry optimization process, the plane-wave cutoff energy of the valence electrons was considered to be set to 350 eV, and a 3 × 3 × 1 Monkhorst-Pack k-mesh is used for the Brillouin zone. The electrostatic potential (ESP) of α-HP_{ace} was calculated using GaussView software package.

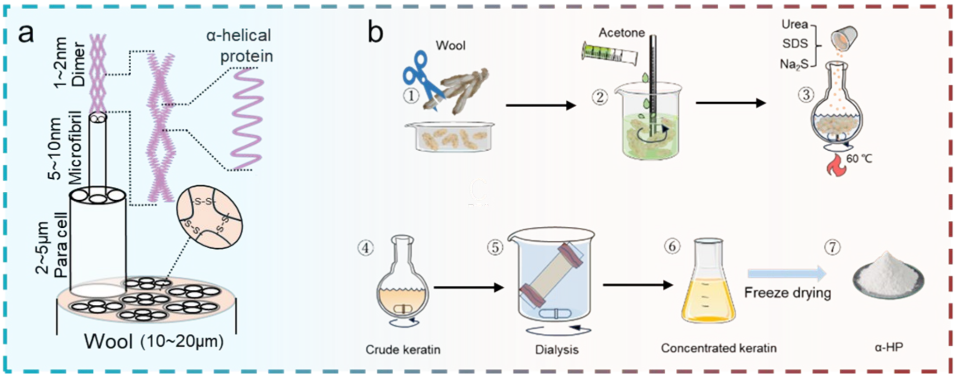

Figure S1. (a) α-helical protein in the wool. (b) The process of protein extraction.

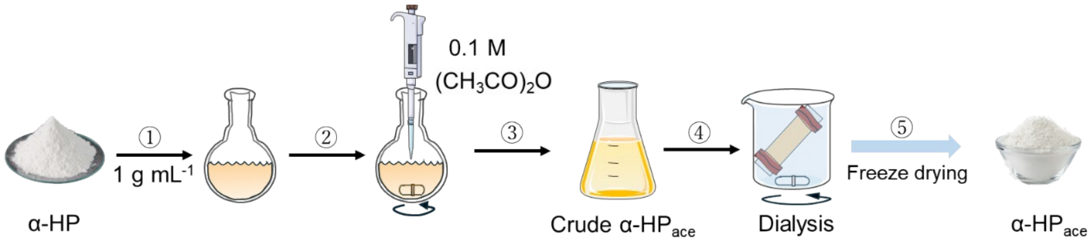

Figure S2. The process of protein acetylation.

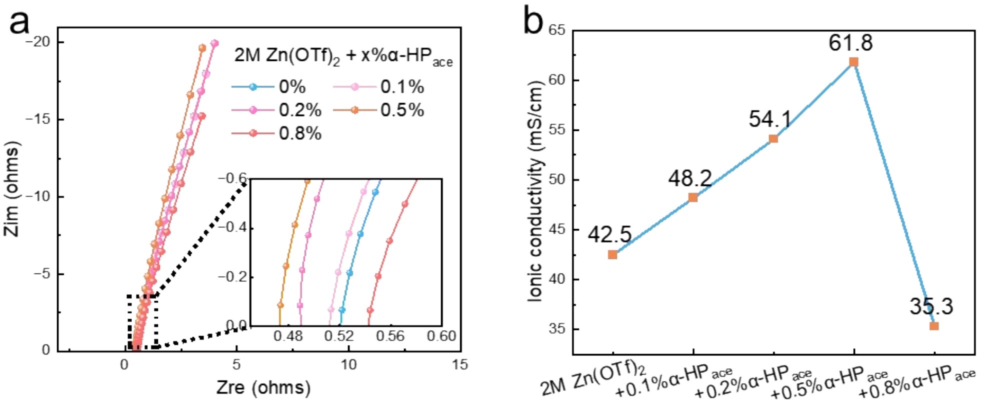

Figure S3. Ionic conductivity of electrolytes with different content of α-HP_{ace}.

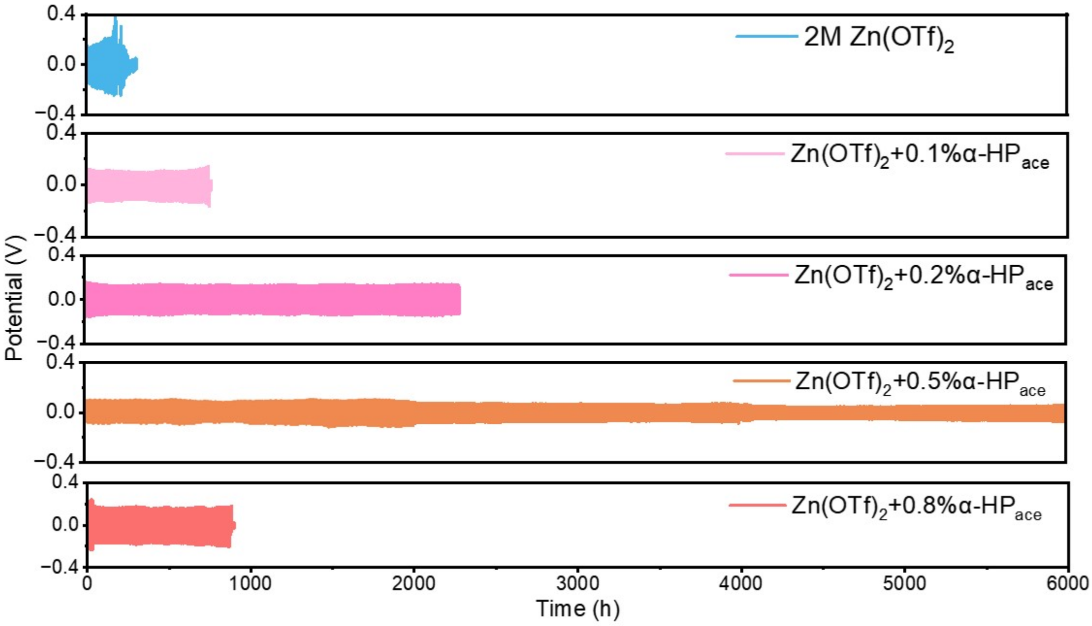

Figure S4. The long-term galvanostatic cycling of symmetric cells with different electrolytes at 1 mA cm^{-2}/1 mAh cm^{-2}.

A electrolyte for bionic ion pumps interface dynamically assembling is obtained by introducing α-HP$_{ace}$ into the 2M Zn(OTf)$_2$ electrolyte (Zn(OTf)$_2$+X%α-HP$_{ace}$, X% denotes the mass percentage of α-HP$_{ace}$ in the electrolyte). As shown in **Figure S3**, the ionic conductivity of the electrolyte first increased and then decreased with the increase of α-HP$_{ace}$ addition (0.1% to 0.8%). The highest ionic conductivity of 61.8 mS/cm can be obtained at an addition amount of 0.5%.High ionic conductivity is the necessary condition to achieve high-performance zinc ion batteries. When the addition amount is increased to 0.8%, the ionic conductivity of the electrolyte decreases to 35.3 mS/cm, which may be attributed to the ionic crowding caused by the interaction of too much α-HP$_{ace}$ with Zn^{2+}.

Zn||Zn symmetric cells assembled with Zn(OTf)$_2$+X%α-HP$_{ace}$ (X=0, 0.1%, 0.2%, 0.5%, and 0.8%) electrolytes are tested for long term constant current cycling at a current density of 1 mA cm^{-2}/1 mAh cm^{-2}. As shown in **Figure S4**, the symmetric cell with Zn(OTf)$_2$+0.5%α-HP$_{ace}$ electrolyte has the longest cycle life with stable cycling of over 6000 h.

In summary, the highest ionic conductivity and the longest cycle life can be obtained with 0.5% α-HP$_{ace}$ addition. The electrolyte obtained with the addition of 0.5% α-HP$_{ace}$ is named α-HP$_{ace}$@Zn(OTf)$_2$. Unless otherwise specified, subsequent appearances of α-HP$_{ace}$@Zn(OTf)$_2$ all represent the electrolyte at this addition amount.

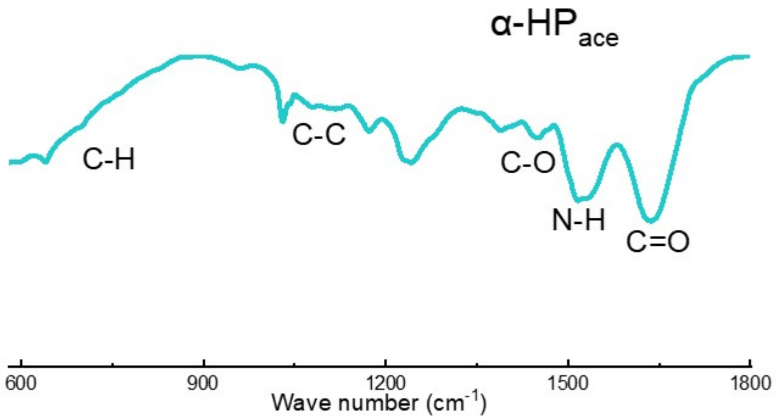

Figure S5. FTIR spectra of α-HP$_{ace}$.

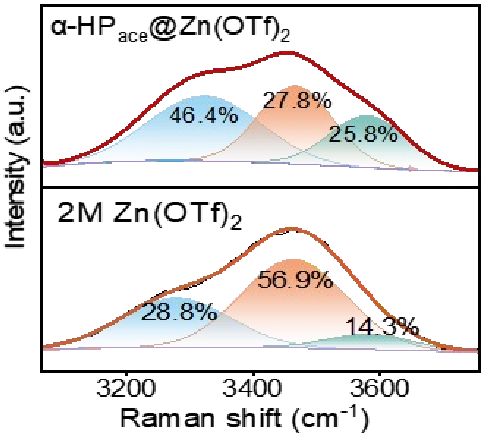

Figure S6. Raman spectra of 2M Zn(OTf)$_2$ and α-HP$_{ace}$@Zn(OTf)$_2$ electrolytes in 2800-3800 cm^{-1}.

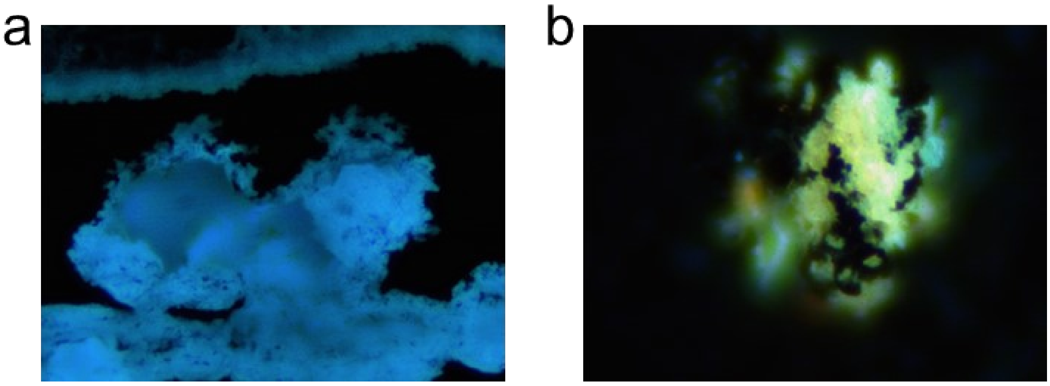

Figure S7. The fluorescent images of Zn anode in protrusion (a) and defect (b).

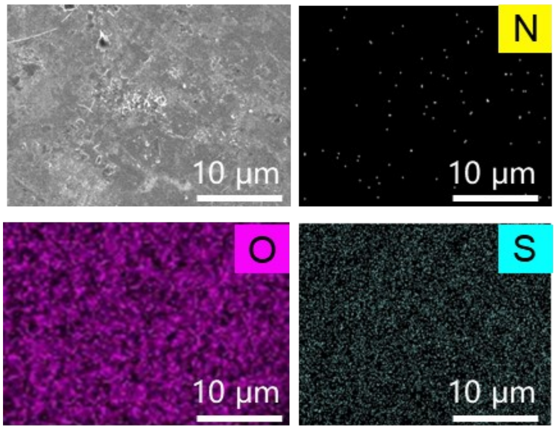

Figure S8. The EDS mapping of Zn anode after soaking in 2M Zn(OTf)$_2$ electrolyte for 2 h.

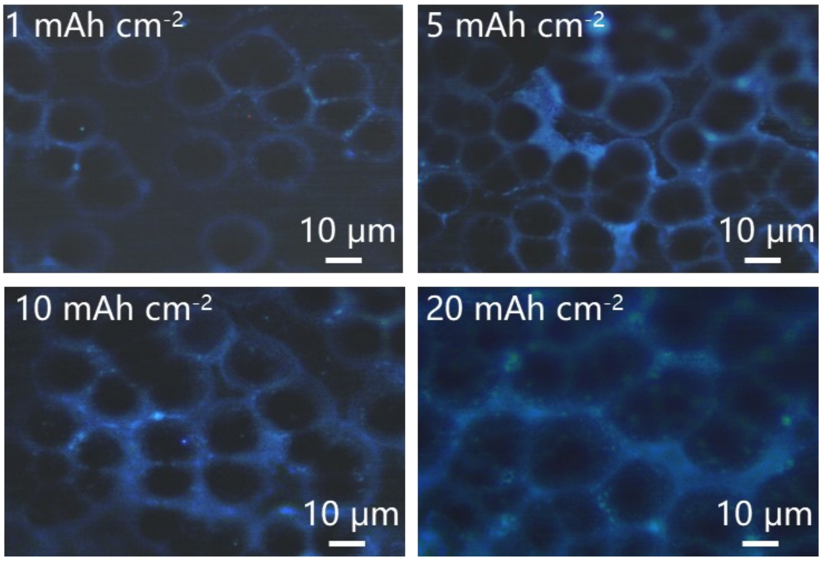

Figure S9. Fluorescence images comparison of Zn@BIPI/α-HP$_{ace}$ anode plated with different Zn capacities.

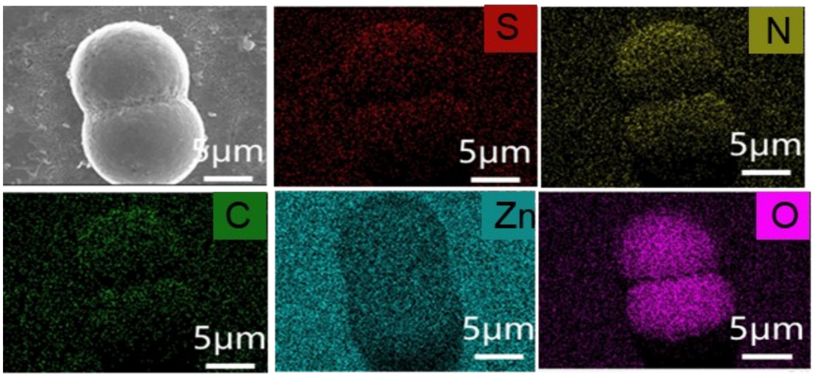

Figure S10. EDS mapping of spherical zinc nuclei planted on Zn@BIPI/α-HP$_{ace}$ anode.

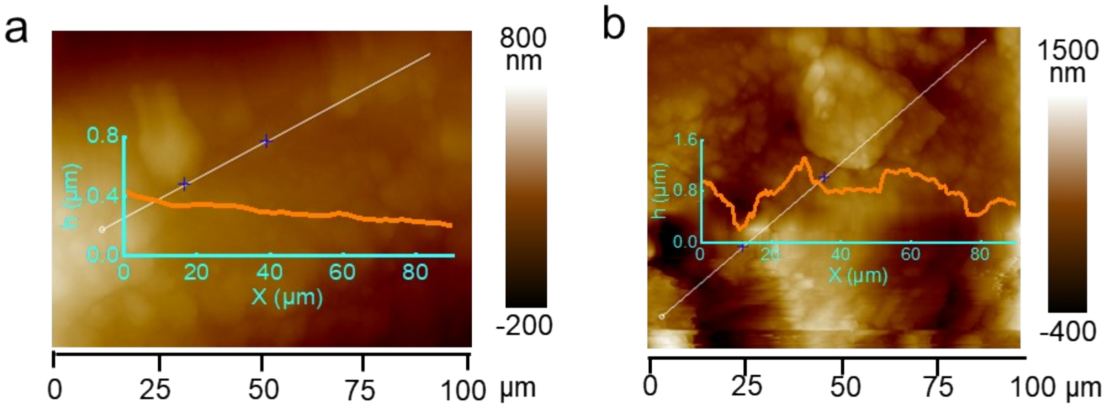

Figure S11. AFM images of the (a) Zn@BIPI/α-HP$_{ace}$ and (b) bare Zn anode surface after plating 20 mAh cm^{-2}.

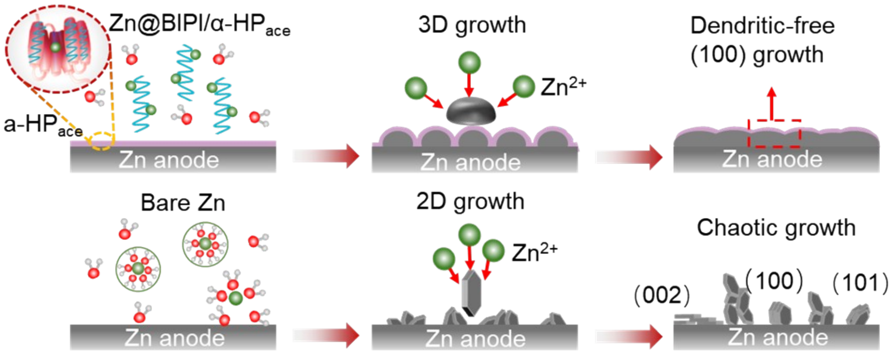

Figure S12. Mechanism diagram of chaotic zinc deposition regulated by α-HP_{ace}.

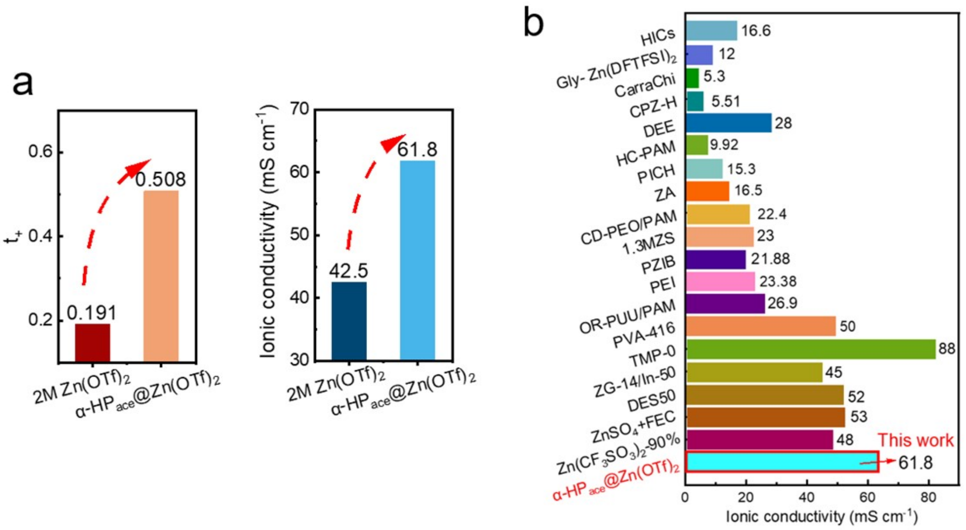

Figure S13. (a) Ion transference number and ionic conductivity of different electrolytes. (b) Comparison of ionic conductivity of electrolytes reported recently.[1-19]

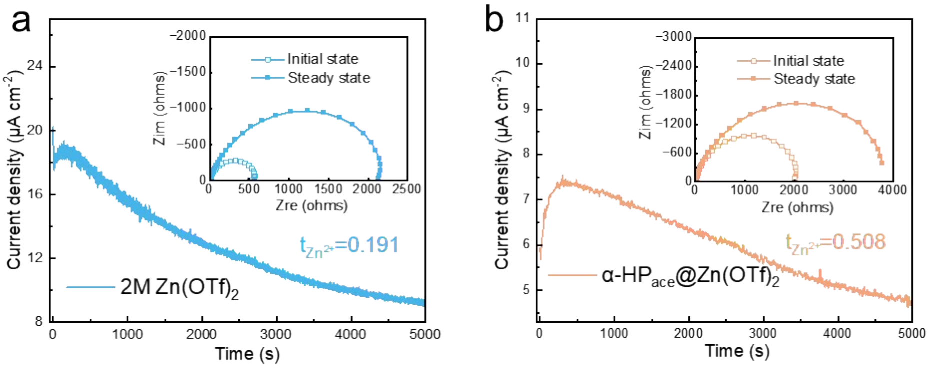

Figure S14. Current variations of the (a) Zn|2M Zn(OTf)$_2$|Zn and (b) Zn|α-HP$_{ace}$@Zn(OTf)$_2$|Zn symmetric cells at room temperature with potentiostatic polarization (ΔV=10 mV). The insert figure is Nyquist plots of symmetric cell at the before potentiostatic polarization (initial state) and after 5000 s of potentiostatic polarization (steady state).

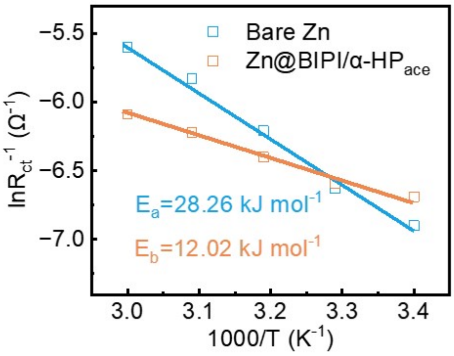

Figure S15. Arrhenius curves and activation energy of bare Zn and Zn@BIPI/α-HP$_{ace}$ anodes.

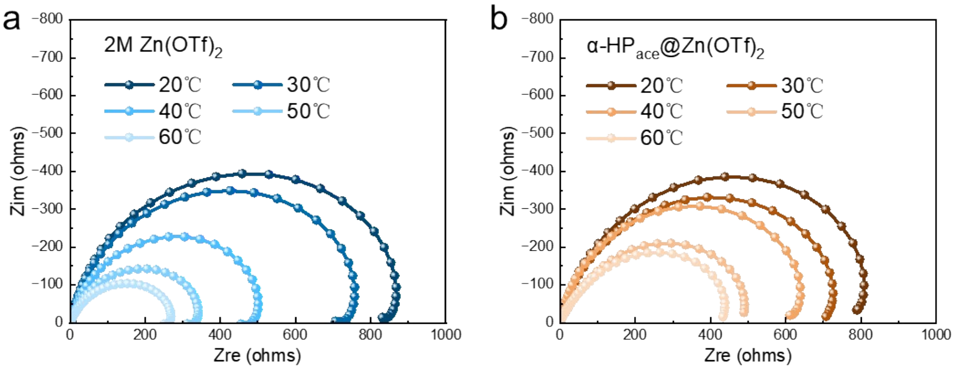

Figure S16. EIS of Zn|2M Zn(OTf)$_2$|Zn (a) and Zn|α-HP$_{ace}$@Zn(OTf)$_2$|Zn (b) symmetric cells at different temperatures.

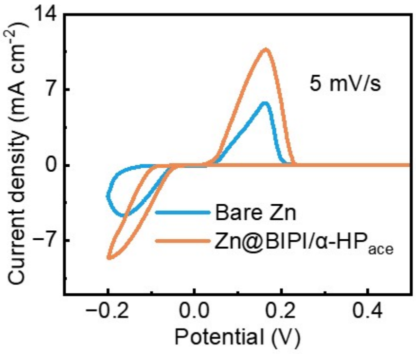

Figure S17. CV curves of bare Zn||Ti and Zn@BIPI/α-HP$_{ace}$||Ti half cells at a scan rate of 5 mV s^{-1}.

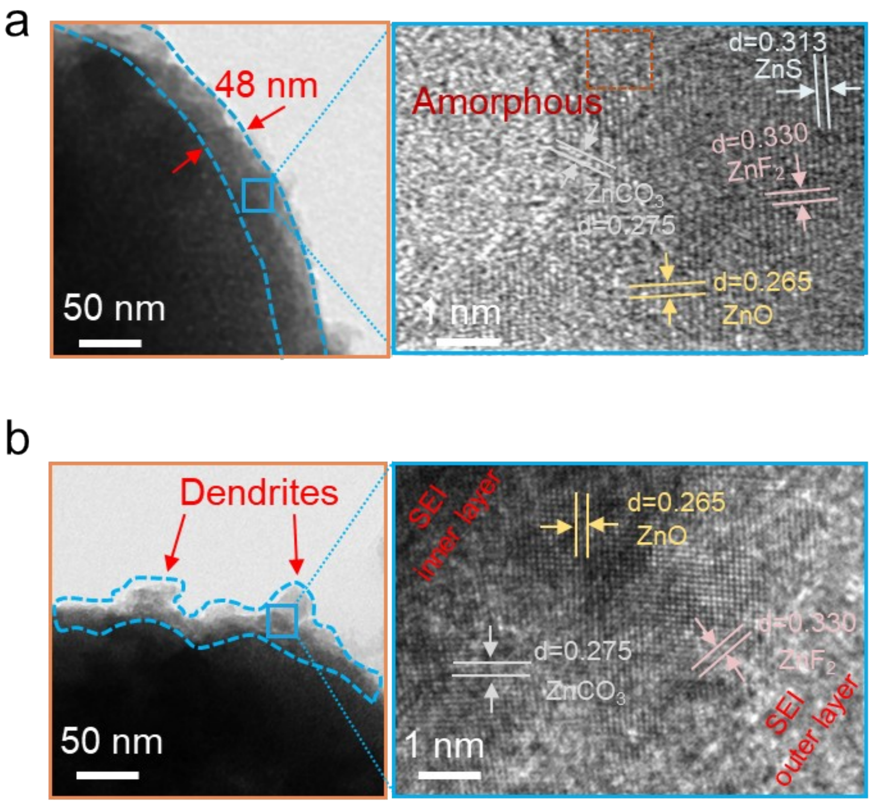

Figure S18. The TEM image and HRTEM magnified images of the (a) Zn@BIPI/α-HP$_{ace}$ and (b) bare Zn anodes after cycling.

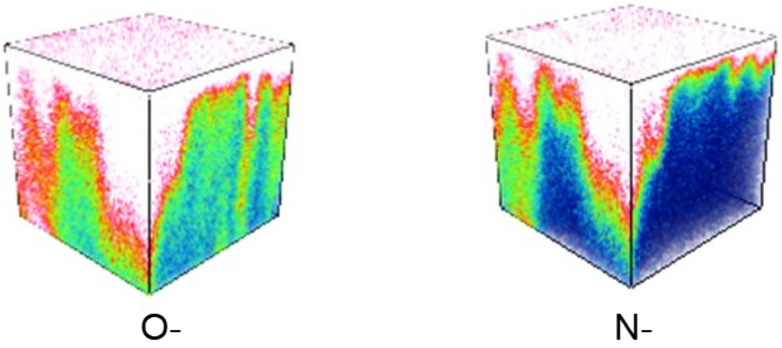

Figure S19. TOF-SIMS 3D view of fragments (O$^-$ and N$^-$) distribution for the Zn@BIPI/α-HP$_{ace}$ anode surface.

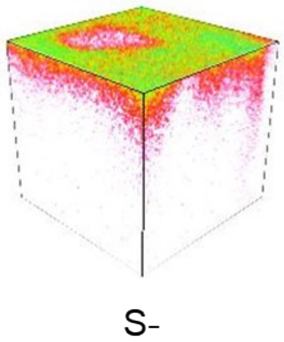

Figure S20. TOF-SIMS 3D view of S$^-$ fragment distribution for the bare Zn anode surface.

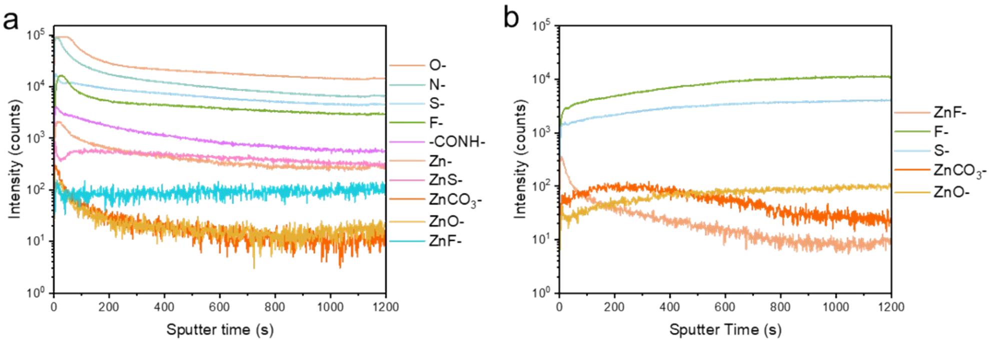

Figure S21. TOF-SIMS depth profiles of (a) Zn@BIPI/α-HP_{ace} and (b) bare Zn anodes after cycling.

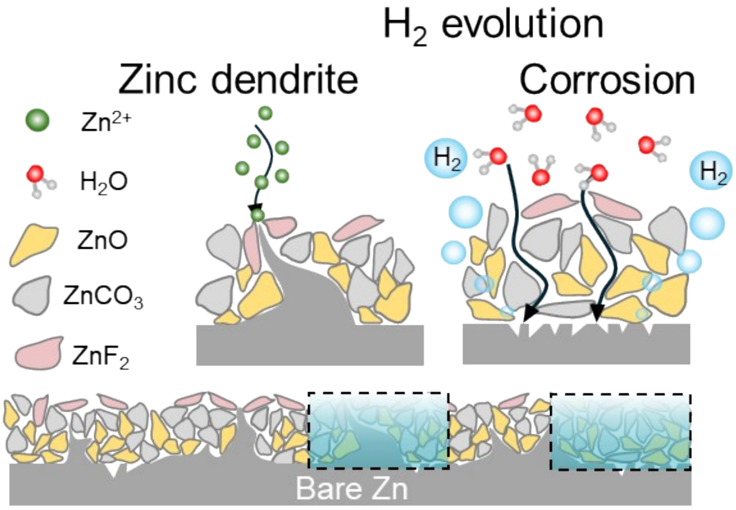

Figure S22. Schematic diagram of SEI on the bare Zn surface, and the issues faced by bare Zn anode.

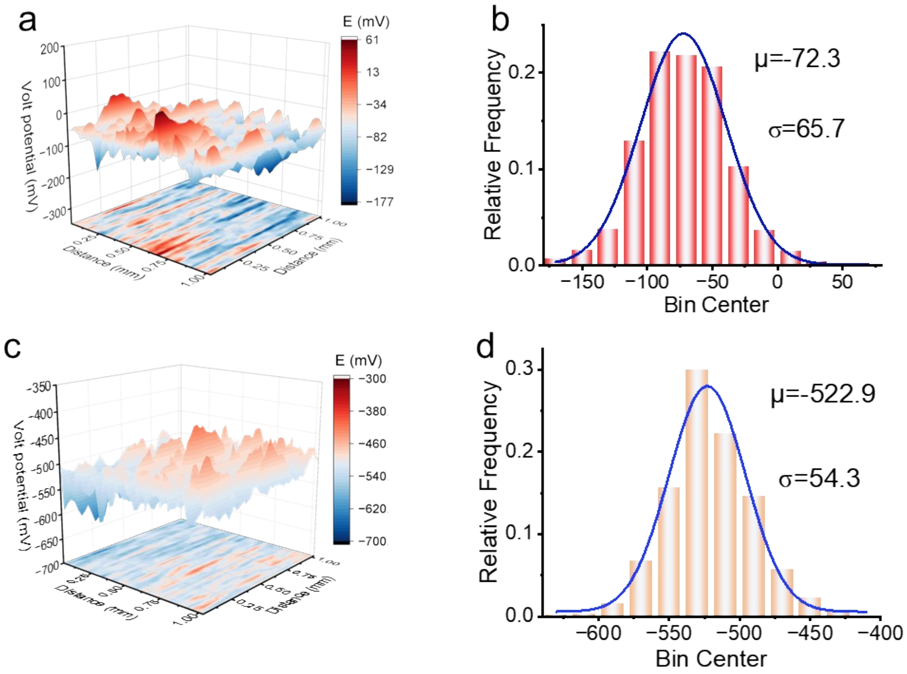

Figure S23. (a) Volta potential maps via SKP testing bare Zn anode after cycling, and (b) the corresponding data statistics of Volta potential by Gaussian fitting. (c) Volta potential maps via SKP testing bare Zn anode at the initial state, and (d) the corresponding data statistics of Volta potential by Gaussian fitting.

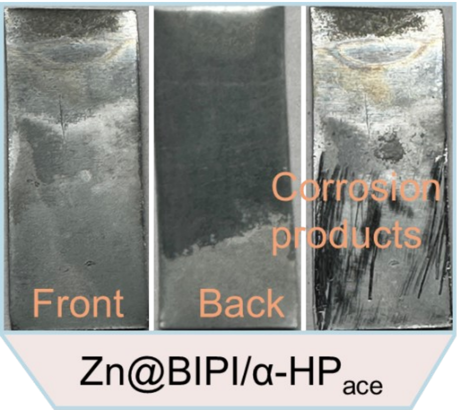

Figure S24. Optical photographs of Zn@BIPI/α-HP$_{ace}$ and bare Zn anodes surface after 30 days immersion in corresponding electrolytes.

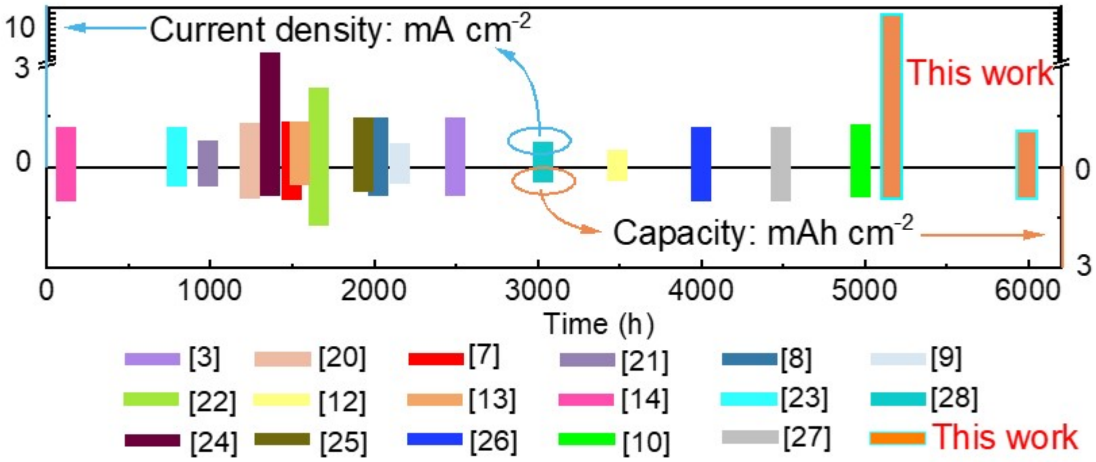

Figure S25. Comparison of cyclic reversibility with cells that have been recently reported.[3, 7-10, 12-14, 20-28].

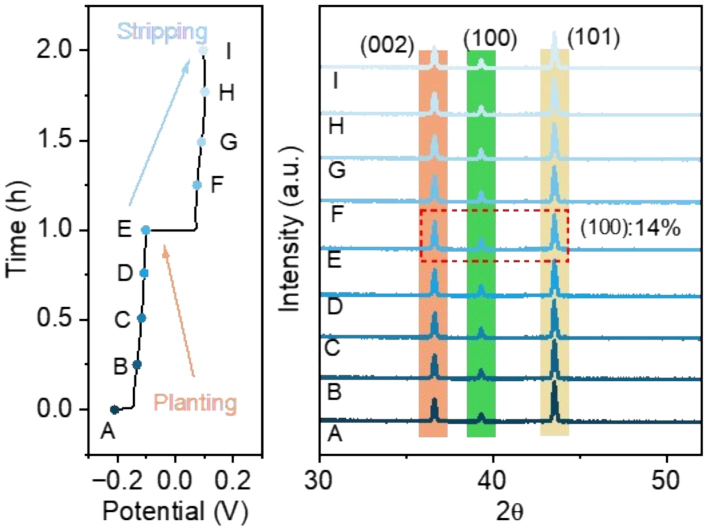

Figure S26. Evolution of ex situ XRD patterns during the Zn plating/stripping process on the bare Zn anode.

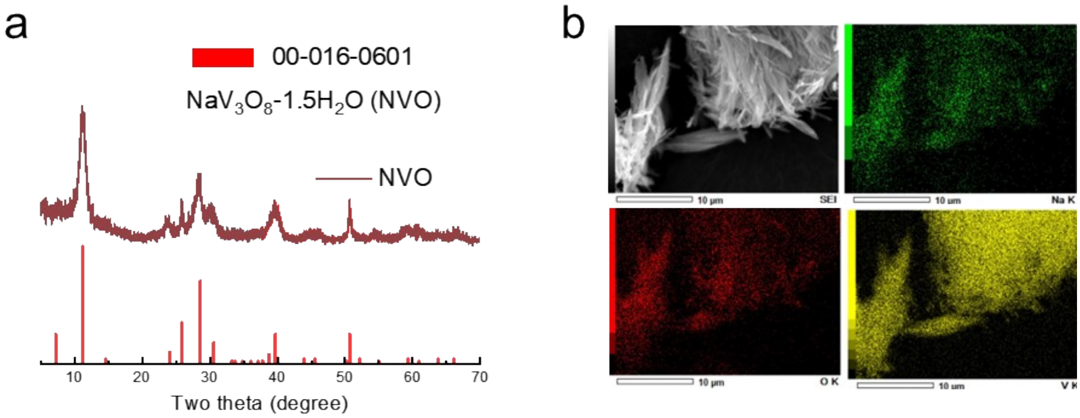

Figure S27. The XRD patterns (a) and SEM image (b) of NVO.

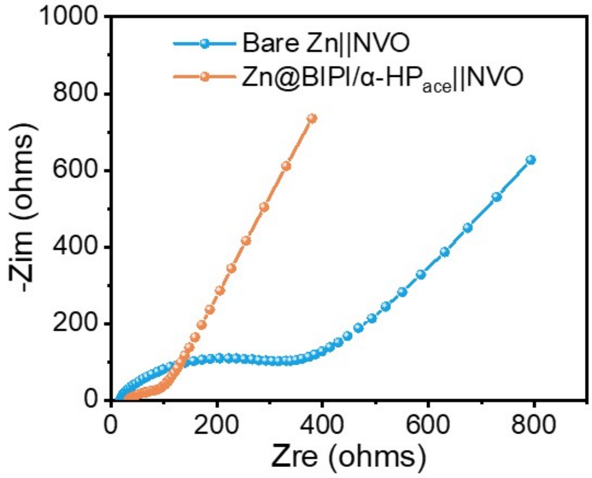

Figure S28. The Nyquist plots of Zn@BIPI/α-HP$_{ace}$||NVO and Zn||NVO full cells.

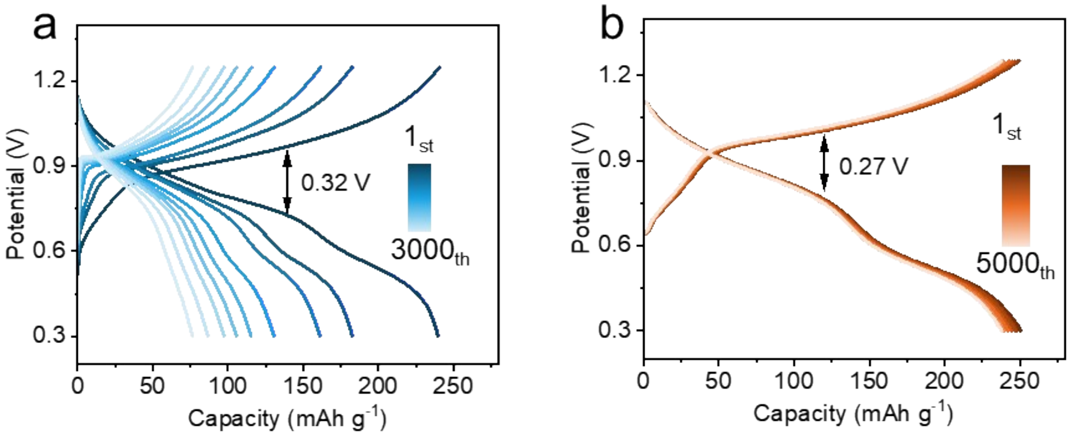

Figure S29. The charge and discharge curves of Zn||NVO (a) and Zn@BIPI/α-HP$_{ace}$||NVO (b) full cells at 5 A g^{-1}.

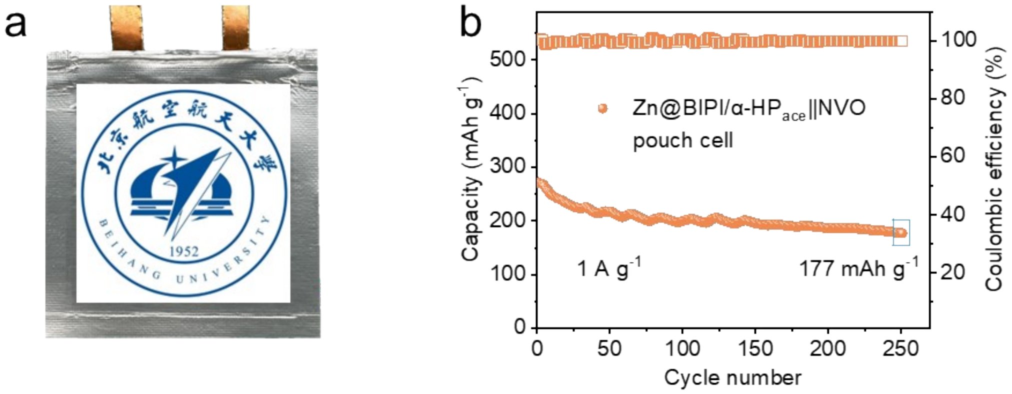

Figure S30. (a) Optical photograph of Zn@BIPI/α-HP$_{ace}$||NVO pouch cell. (b) The long-term cycling performance of Zn@BIPI/α-HP$_{ace}$||NVO pouch cell at 1 A g^{-1}.

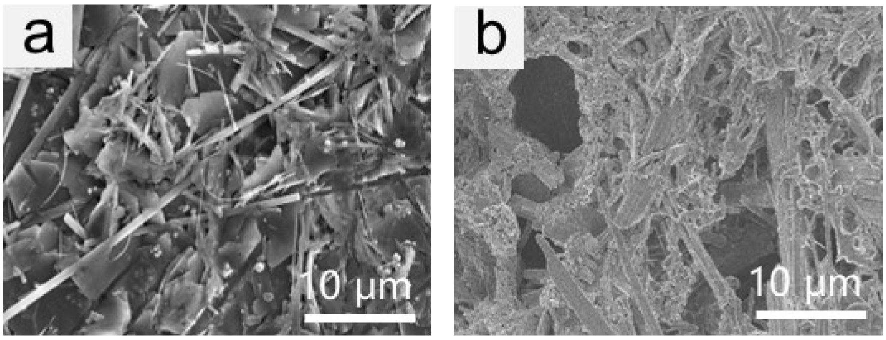

Figure S31. The SEM images of bare Zn anode (a) and NVO cathode (b) in Zn||NVO full cell after cycling at 5 A g^{-1}.

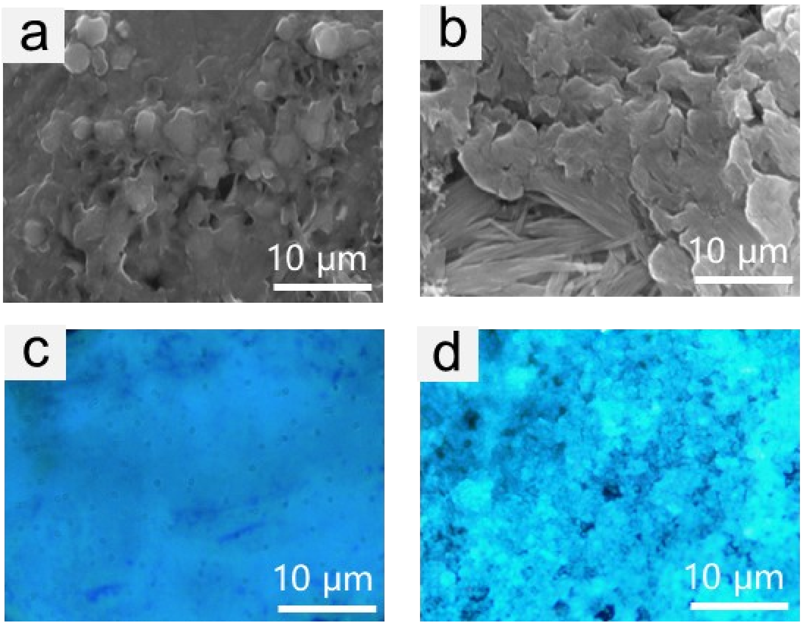

Figure S32. The SEM images and fluorescent photographs of Zn@BIPI/α-HP$_{ace}$ anode (a, c) and NVO cathode (b, d) in Zn@BIPI/α-HP$_{ace}$||NVO full cell after cycling at 5 A g^{-1}.

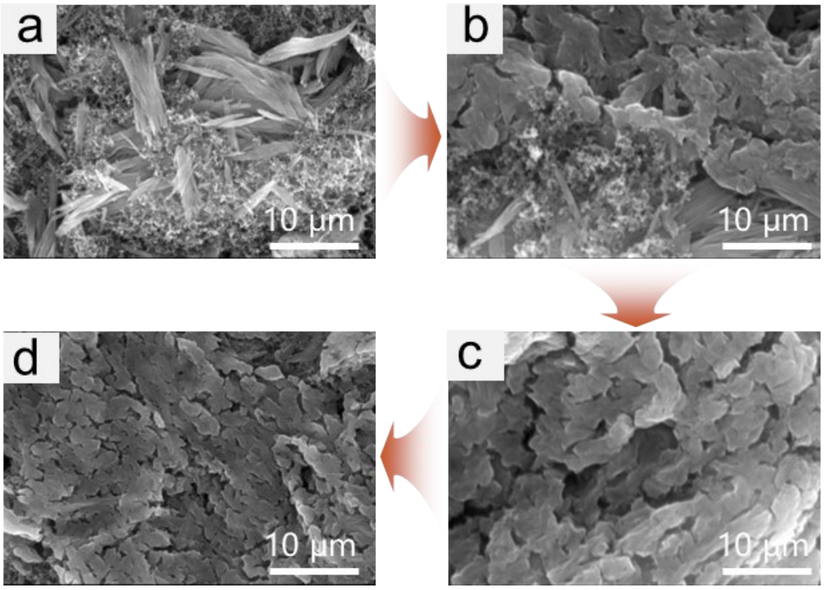

Figure S33. SEM images of NVO cathode after cycling in Zn@BIPI/α-HP$_{ace}$||NVO full cell with different cycles. (a) 1 cycle. (b) 5 cycles. (c) 10 cycles. (d) 20 cycles.

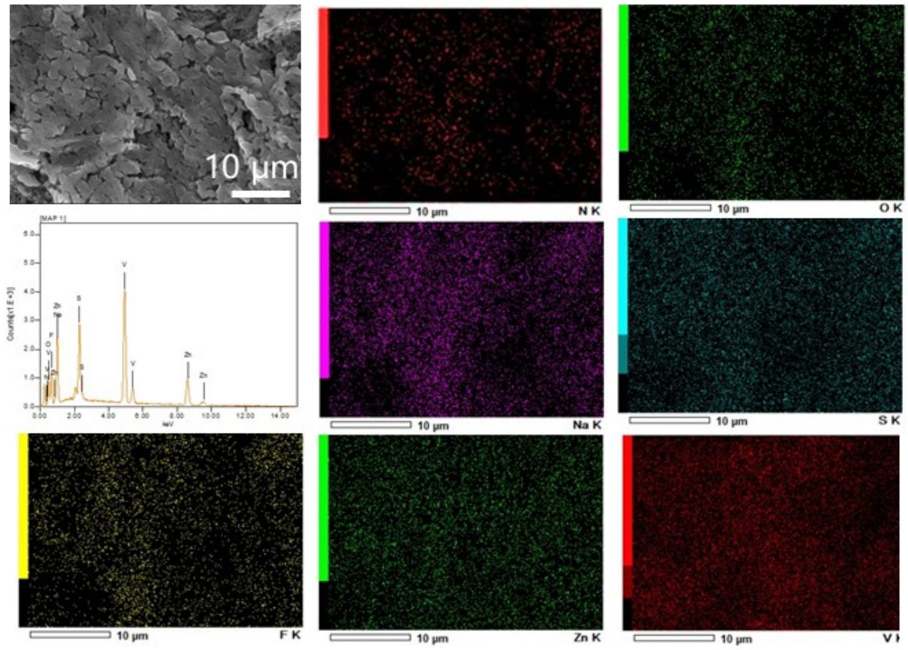

Figure S34. EDS mapping of NVO cathode after cycling in Zn@BIPI/α-HP$_{ace}$||NVO full cell with 20 cycles.

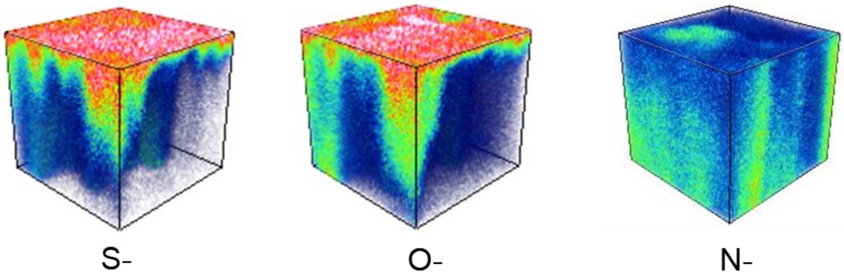

Figure S35. TOF-SIMS 3D view of fragments distribution for the NVO cathode surface cycled in Zn@BIPI/α-HP$_{ace}$||NVO full cell.

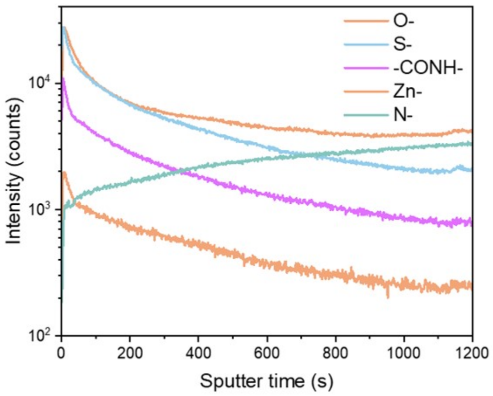

Figure S36. TOF-SIMS depth profile of NVO cathode after cycled in Zn@BIPI/α-HP$_{ace}$||NVO full cell.

Supplemental References

1 X. Y. Wang, Y. R. Ying, S. M. Chen, Q. J. Meng, H. T. Huang, L. T. Ma, *Nano Energy*. 2024, **119**, 109099.

2 Y. Yan, S. Duan, B. Liu, S. Wu, Y. Alsaid, B. Yao, S. Nandi, Y. Du, T. W. Wang, Y. Li, X. He, *Adv. Mater*. 2023, 2211673.

3 F. F. Wang, J. P. Zhang, H. T. Lu, H. B. Zhu, Z. H. Chen, L. Wang, J. Y. Yu, C. H. You, W. H. Li, J. W. Song, Z. Weng, C. P. Yang, Q. H. Yang, *Nat Commun*. 2023, **14**, 4211.

4 H. Y. Lu, J. S. Hu, X. J. Wei, K. Q. Zhang, X. Xiao, J. X. Zhao, Q. Hu, J. Yu, G. M. Zhou, B. G. Xu, *Nat Commun*. 2023, **14**, 4435.

5 S. M. Chen, S. M. Li, L. T. Ma, Y. R. Ying, Z. X. Wu, H. T. Huang, C. Y. Zhi, *Angew. Chem., Int. Ed*. 2024, **63**, e202319125.

6 H. H. Y. Wang, Y. Q. Zhang, B. Han, Q. Li, X. Guo, Y. Guo, A. Chen, Z. Q. Wei, Z. D. Huang, Y. W. Zhao, J. Fan, C. Y. Zhi, *Adv. Mater*. 2024, 2407150.

7 Y. Hao, D. D. Feng, L. Hou, T. Y. Li, Y. C. Jiao, P. Y. Wu, *Adv. Sci*. 2022, **9**, 2104832.

8 K. P. Zhu, J. Luo, D. H. Zhang, N. Y. Wang, S. B. Pan, S. J. Zhou, Z. J. Zhang, G. D. Guo, P. Yang, Y. Fan, S. S. Hou, Z. P. Shao, S. Z. Liu, L. Lin, P. Xue, G. Hong, Y. R. Yang, Y. G. Yao, *Adv. Mater*. 2024, 2311082.

9 Z. F. Yang, Q. Zhang, T. Q. Wu, Q. K. J. M. Li, J. Q. Gan, S. E. Xiang, H. Wang, C. Hu, Y. G. Tang, H. Y. Wang, *Angew. Chem., Int. Ed*. 2024, **63**, e202317457.

10 J. L. Yang, T. Xiao, T. Xiao, J. Li, Z. H. Yu, K. Liu, P. H. Yang, H. J. Fan, *Adv. Mater.* 2024, **36**, 2313610.

11 Z. X. Liu, Z. Z. Chen, S. R. Lei, B. G. Lu, S. Q. Liang, J. J. Li, J. Zhou, *Adv. Mater*. 2024, 2308836.

12 Q. B. Liu, X. Ou, Y. J. Niu, L. G. Li, D. D. Xing, Y. J. Zhou, F. Yan, *Angew. Chem., Int. Ed*. 2024, e202317944.

13 C. W. Li, W. H. Wang, J. Luo, W. B. Zhuang, J. X. Zhou, S. Z. Liu, L Lin, W. B. Gong, G. Hong, Z. P. Shao, J. M. Du, Q. C. Zhang, Y. G. Yao, *Adv. Mater*. 2024, 2313772.

14 H. Xia, G. Xu, X. Cao, C. Y. Miao, H. N. Zhang, P. Y. Chen, Y. Zhou, W. Zhang, Z. M. Sun, *Adv. Mater*. 2023**, 35**, 2301996.

15 S. J. Zhang, J. Hao, Y. Zhu, H. Li, Z. Lin, S. Qiao, *Angew. Chem., Int. Ed*. 2023, e202301570.

16 D. Xie, Y. Sang, D. H. Wang, W. Y. Diao, F. Y. Tao, C. Liu, J. W. Wang, H. Z. Sun, J. P. Zhang, X. L. Wu, *Angew. Chem., Int. Ed*. 2023, **135**, e202216934.

17 S. H. Wang, G. X. Liu, W. Wan, X. Y. Li, J. Li, C. Wang, *Adv. Mater.* 2024, **36**, 2306546.

18 J. D. Wan, R. Wang, Z. X. Liu, S. L. Zhang, J. N. Hao, J. F. Mao, H. B. Li, D. L. Chao, L. H. Zhang, C. F. Zhang, *Adv. Mater*. 2023, 2310623.

19 W. Wang, S. Chen, X. L. Liao, R. Huang, F. M. Wang, J. L. Chen, Y. X. Wang, F. Wang, H. Wang, Nat Commun. 2023, **14**, 5443.

20 M. Li, C. Xi, X. Wang, L. Li, Y. Xiao, Y. Chao, X. Zheng, Z. Liu, Y. Yu, C. Yang, *Small* 2023, 2301569.

21 X. Lin, G. Zhou, J. Liu, M. J. Robson, J. Yu, Y. Wang, Z. Zhang, S. C. T. Kwok, F. Ciucci, *Adv. Funct. Mater*. 2021, **31**, 2105717.

22 H. Wang, A. Zhou, Z. Hu, X. Hu, F. Zhang, Z. Song, Y. Huang, Y. Cui, Y. Cui, L. Li, F. Wu, R. Chen, Angew. Chem. Int. Ed. 2024, 63, e202318928.

23 X. Fan, H. Wang, X. Liu, J. Liu, N. Zhao, C. Zhong, W. Hu, J. Lu, *Adv. Mater*. 2023, **35**, e2209290.

24 W. Zhong, Z. Shen, J. Mao, S. Zhang, H. Cheng, Y. Kim, Y. Lu, *Energy Environ. Sci*. 2024, **17**, 2059.

25 Z. Zheng, X. Zhong, Q. Zhang, M. Zhang, L. Dai, X. Xiao, J. Xu, M. Jiao, B. Wang, H. Li, Y. Jia, R. Mao, G. Zhou, *Nat. Commun*. 2024, **15**, 753.

26 F. Zhang, T. Liao, H. Peng, S. Xi, D.-C. Qi, A. Micallef, C. Yan, L. Jiang, Z. Sun, *J. Am. Chem. Soc*. 2024, **146**, 10812.

27 Q. Wu, J. Huang, J. Zhang, S. Yang, Y. Li, F. Luo, Y. You, Y. Li, H. Xie, Y. Chen, *Angew. Chem. Int. Ed*. 2024, e202319051.

28 B. Liu, C. Wei, Z. Zhu, Y. Fang, Z. Bian, X. Lei, Y. Zhou, C. Tang, Y. Qian, G. Wang, *Angew. Chem. Int. Ed*. 2022, **61**, e202212780.